Functional Composite-Based Wireless Sensing Platform for Bridge Structures

Chenglin Wu, PhD
Associate Professor
Department of Civil, Architectural, and
Environmental Engineering
Missouri University of Science and Technology

Xanxiao Li, PhD
Postdoctoral Research Scientist
NETL Support Contractor
National Energy Technology Laboratory, US DOE

2024

Functional Composite-Based Wireless Sensing Platform for Bridge Structures

Chenglin Wu, Ph.D.
Associate Professor
Civil and Environmental Engineering
Texas A&M University

Yanxiao Li, Ph.D.
Postdoctoral Research Scientist
NETL Support Contractor, National Energy
Technology Laboratory, U.S. DOE

A Report on Research Sponsored by

Mid-America Transportation Center

University of Nebraska–Lincoln

September 2024

Technical Report Documentation Page

1. Report No. 25-1121-0005-129-2	2. Government Accession No.	3. Recipient's Catalog No.	
4. Title and Subtitle Functional Composite-Based Wireless Sensing Platform for Bridge Structures		5. Report Date September 2024	
		6. Performing Organization Code	
7. Author(s) Chenglin Wu, 0000-0001-7733-1084 Yanxiao Li,		8. Performing Organization Report No. 25-1121-0005-129-2	
9. Performing Organization Name and Address Missouri University of Science and Technology, 1401 N. Pine St., Rolla, MO		10. Work Unit No. (TRAIS)	
		11. Contract or Grant No. 69A3551747107	
12. Sponsoring Agency Name and Address Office of the Assistant Secretary for Research and Technology 1200 New Jersey Ave., SE Washington, D.C. 20590		13. Type of Report and Period Covered Final Report January 2020 – June 2024	
		14. Sponsoring Agency Code MATC TRB RiP No. 91994-50	
15. Supplementary Notes N.A.			

16. Abstract

The main objective of this research is to develop and deploy a wireless crack sensing system that can measure and monitor cracks for both concrete and steel bridge structures. This system will contain the sensing unit, wireless data transmitting system, as well as a data processing unit. The sensing unit will consist of single or arrays of advanced thin film-based sensing nodes that are capable to measuring crack induced strains in bridge structures. This thin film sensing node contains soft polymer film (polyvinylidene difluoride, PVDF) embedded with conductive nanoparticles (graphene) or atomically thin films. Both the Poisson's effect and contact mechanism will be considered to covert the strain to electrical resistance of the sensing unit. This sensing unit is also connected to a wireless transmitting system to broadcast the signal wirelessly. The wireless transmitting system utilizes a blue-tooth technology that can enable the sensing unit to broadcast electronic signals in terms of electrical resistance. These signals were received by a mobile device (laptop or cellphone) that can convert the electrical resistance information into the measured stains. These measurements are processed using the data processing unit. The data processing unit will receive the electrical resistance data and convert it into measured strains. The machine learning approach was also taken to train the software to be able to automatically detect the abnormalities in the measured strain for critical crack growth detection.

17. Key Words Wireless crack sensors, graphene, bridges		18. Distribution Statement	
19. Security Classif. (of this report) Unclassified	20. Security Classif. (of this page) Unclassified	21. No. of Pages 47	22. Price

Table of Contents

List of Figures

Executive Summary

The main objective of this research is to develop and deploy a wireless crack sensing system that can measure and monitor cracks for both concrete and steel bridge structures. This system will contain the sensing unit, wireless data transmitting system, as well as a data processing unit. The sensing unit will consist of single or arrays of advanced thin film-based sensing nodes that are capable of measuring crack-induced strains in bridge structures. These thin film sensing nodes contain soft polymer film (polyvinylidene difluoride, PVDF) embedded with conductive nanoparticles (graphene) or atomically thin films. Both the Poisson's effect and contact mechanism will be considered to convert the strain to electrical resistance of the sensing unit. This sensing unit is also connected to a wireless transmitting system to broadcast the signal wirelessly. The wireless transmitting system utilizes Bluetooth technology that can enable the sensing unit to broadcast electronic signals in terms of electrical resistance. These signals were received by a mobile device (laptop or cellphone) that can convert the electrical resistance information into the measured stains, which can then be processed using the data processing unit. The data processing unit will receive the electrical resistance data and convert it into measured strains. A machine learning approach was also used to train the software to be able to automatically detect the abnormalities in the measured strain for critical crack growth detection.

Keywords: Bridge; Cracking; Sensor; Nanocomposite; Graphene: Raspberry Pi, Cloud, Machine learning

Chapter 1 Introduction

1.1 Problem Statement

1.1.1 Corrosion and cracking

Corrosion is one of most critical reliability issues of our crumbling civil infrastructure as shown in Figure 1.1(a-c). The annual budget for repairs and maintenances caused by corrosion is about $1 trillion, based off a starting point of $276 billion in 1998 and using 2013's inflation estimate. The actual cost paid is expected to be at least $552 billion [1] as illustrated in Figure 1.1(d). In addition, corrosion induced structural cracking and failures are most common for bridge structures constructed either with structural steel or reinforced concrete, which can cause catastrophic failures that may lead to loss of human lives. Therefore, monitoring corrosion induced strain and failures and providing timely warnings are essential to the daily operations of transportation infrastructure.
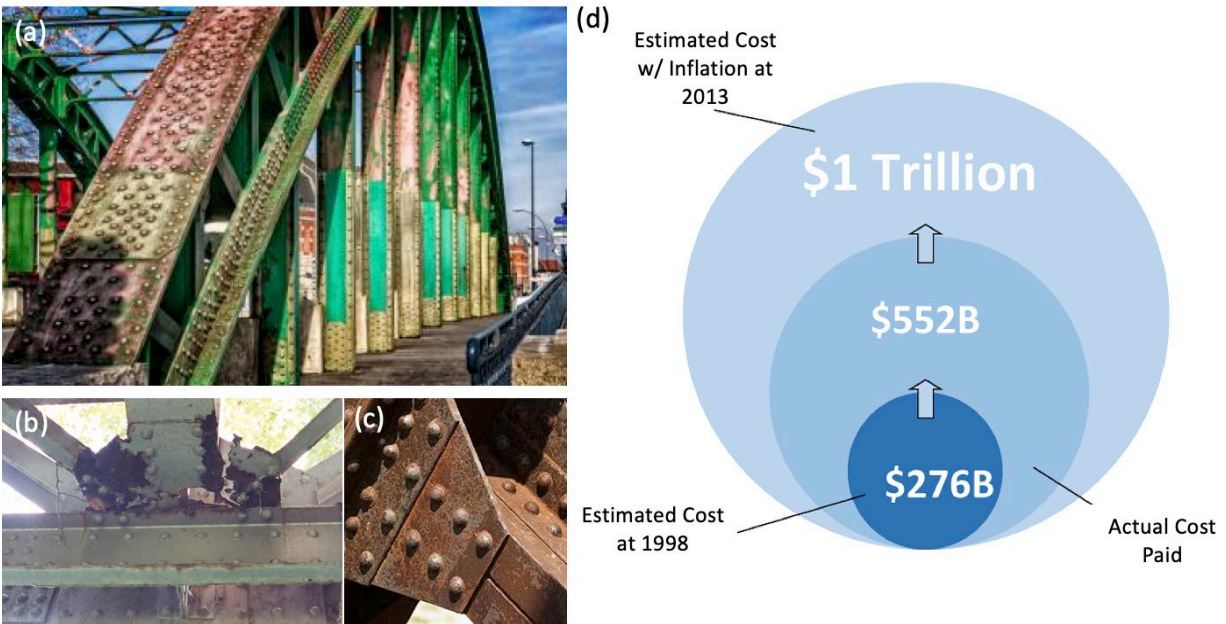
Figure 1.1 (a)-(c) Corrosion induced structural failures for steel bridges; (d) associated cost in repairs [1].

1

1.1.2 Existing sensing approaches

Two main approaches have been commonly taken to develop such systems: (1) fiber-optic sensors and (2) electrical-resistance based sensing devices. However, due to the size limitation on the spectrum scope as well as the required continuous length, it is extremely challenging to fabricate a compact, portable, and wireless fiber-optic sensor.

On the other hand, the electrical-resistance based sensor can be downsized, making them ideal candidates for the next-generation wireless sensing platform. Although the commercially available strain sensors cannot satisfy the critical requirement for crack sensing, which is to have both the high resolution and large sensing range simultaneously without enlarging the sensor size. The drawback is rooted in the basic design of the commercially available strain gauges (typically metal foil) as illustrated in Figure 1.2. By embedding a thin metal coil in the hard polymer substrate, this type of strain gauge relies on the relatively small stretching of the coil segments within each grid length to amplify the changes of electrical resistance. Due to the high sensitivity of metal to straining, a high resolution in terms of strain measurements can be achieved. However, for a relatively large strain, which is often time observed in crack sensing, this design loses its appeal due to the low failure strain of the metal coils.
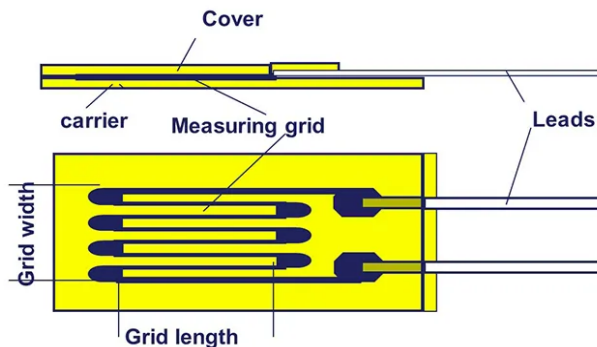
Figure 1.2 Design of a typical metal foil strain gauge [2].

2

To overcome this shortcoming, the mechanical sensors have been widely used for crack measurements. One of the most adopted mechanical sensors is the extensometers as illustrated in Figure 1.3. These mechanical strain gauges utilize the levers to mechanically magnify the cracking within the gauge length to achieve better resolutions. Although these devices are relatively reliable and have the range of measurements needed, their need for installation and vulnerability to environmental conditions (rain, moisture, and low temperatures) make them impossible to use for long-term crack sensing and monitoring.
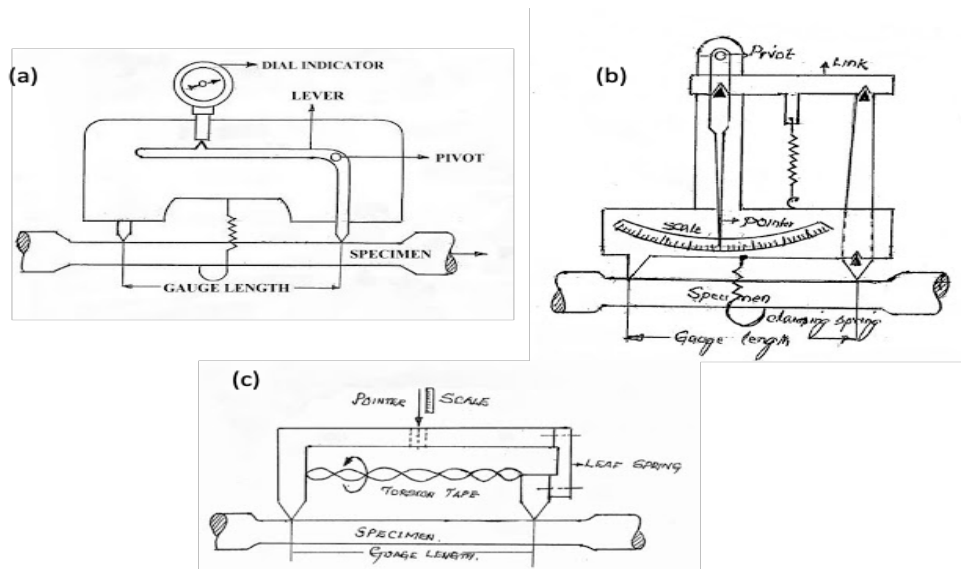
Figure 1.3 Design of typical mechanical strain gauge (extensometers): (a) Berry, (b) Huggenbeger, (c) Johansson [3].

Certainly, there are other types of crack sensing including the non-contact image-based measurements [4]. However, these image-based methods have high requirements for lighting conditions, surface textures, as well as image acquisition equipment.

1.1.3 Proposed sensing materials and mechanisms

To overcome the challenge to find a new sensing approach for cracks that offers both high resolution and long-range measurements, we turn our attention to the rapidly functional soft materials. Active or functional soft materials are often times polymeric composites that have functional fillings to achieve exceptional electrical, optical, or magnetic properties. Early adaptations of the materials explored the combination of carbon black particles deposited on rubbery substrates [5]. However, the relatively large carbon black particles and difficulties of achieving uniform mixes pose challenges in consistency during large-scale applications. With the rapid growth of nanotechnology, graphene has emerged as wonder material, which has exceptional conductivity, dispersion capability, as well as durability for sensing applications [6]. For the matrix materials, PVDF has drawn a tremendous amount of attention due to its interesting piezoelectric properties. Polyvinylidene difluoride (PVDF) is a thermoplastic polymer with a semicrystalline microstructure and a varied polymorphism, showing high compliance, thermal and chemical stability, and piezoelectric and pyroelectric properties. These properties are the base of different applications such as tactile sensors, infrared imaging devices, actuators, electrolyte-gated transistors, etc. [7]. The incorporation of different nanofillers is a way to further improve the performance of raw PVDF and extend its applications (fig. 1.4). In this project, we utilized the graphene as the nanofillers to create network structure. This conductive network structure offers two sensing mechanisms: (1) the piezoresistive mechanism, where the stretching of the PVDF matrix will change the internal contact of graphene flakes leading to changed electrical resistance, and (2) the piezoelectrical mechanism, where the local electrical field generated by the networked graphene structure will also offer change of resistance. We found that the piezoresistive mechanism is dominant due to an almost linear relationship between the straining and electrical

resistance, which is convenient for the proposed crack sensing. In addition, the inherently large

deforming capability of PVDF offers the possibility for the required large cracking strain.
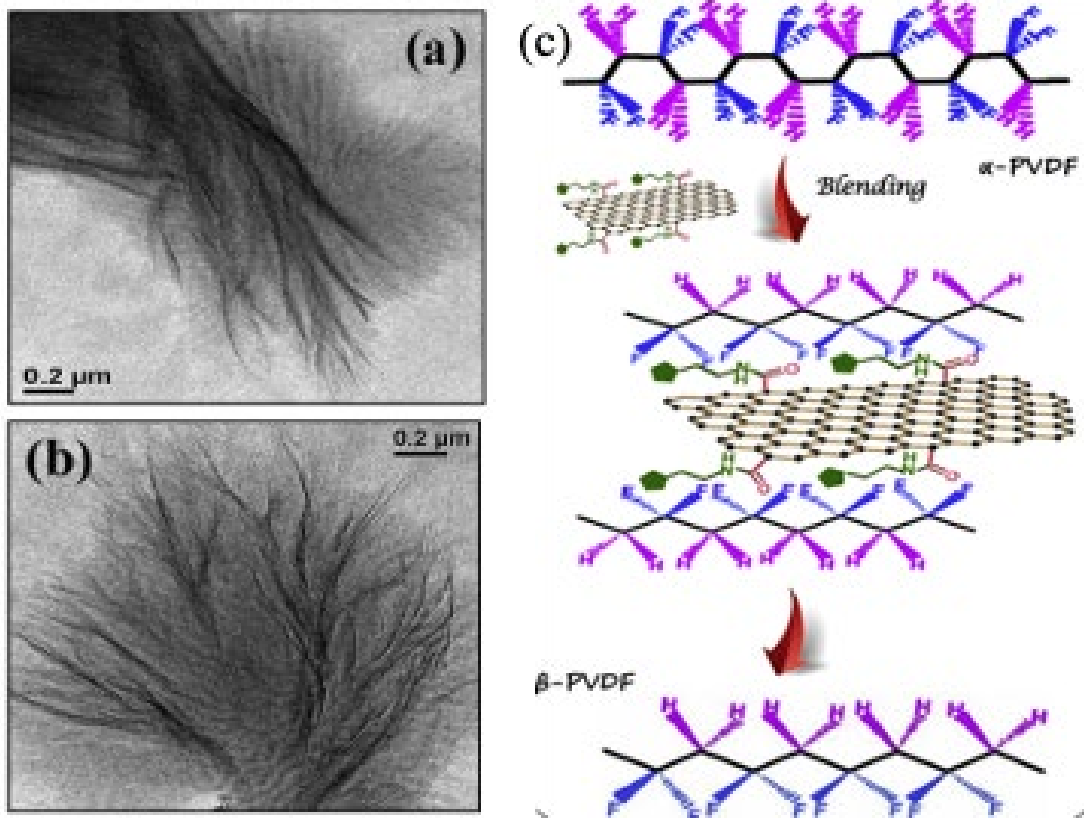
Figure 1.4 (a) (b) TEM images of PVDF-graphene with different concentration of graphene oxides; (c) Molecular structures of reduced graphene oxides with PVDF [8]

1.1.4 Data transmission, crack growth warning, and self-efficient energy system

For the data transmission system, we will need a portable, integrated computer device that

can effectively receive, process, and analyze the strain data as well as detect and track the

abnormality of the data. The ideal system should also be low cost and have low power consumption

so that it will be affordable for large scale applications. To achieve this, we selected the recently

released Raspberry Pi systems [9], which offers both features in addition to flexibility features in integrating multicomponents of electrical hardware and software.

For the data processing, we need a real-time, automatic "processer", that can review the strain data, process the data, and understand the trend of the data to establish a baseline for normality. When an incident (such as sudden crack growth) occurs, this "processer" can detect and send corresponding messages to bridge engineers. A human processer would be ineffective for long-term monitoring, as well as costly. This leads to the incorporation of a recently developed machine learning approach. In this project, we utilized the deep artificial neural network (ANN) approach to establish the data normality. For the case study, we installed the sensing system to the exterior railing of a residential building to understand the thermal straining phenomenon. When an incident such as sudden impact occurs, we will observe a sudden increase of strain, which can then be detected by the trained ANN approach. This provides the potential solution to the crack growth warning issue. Finally, we also need to reduce the entire system to run on a small capacity energy storage device (e.g., a 9-volt battery), which should be able to be charged with a solar panel to achieve self-energy efficiency for the targeted long-term monitoring.

1.2 General approaches, challenges, solutions, and tasks

From the literature study and rationalization presented in Section 1.1, we have decided to utilize the PVDF polymer matrix and graphene nanofillers to make the soft piezoresistive sensor, which is capable of large deformations with high strain to electrical signal sensitivity. We also decided to utilize Raspberry Pi devices to integrate the data acquisition, processing, and wireless transmission. We will utilize machine learning to further process the data, learn the normal strain variation trend and detect abnormal strain readings. Combining these three techniques, we are expected to deliver a novel sensing system that can wirelessly sense crack, detect crack growth,

6

and alert engineers in real time. Despite the promise, there are several critical questions needing answered from the application aspects:

(1)   Can we achieve low cost, large scale processing to deliver high quality of graphene needed for the sensor fabrication?

(2)   Does the microstructure of the sensor matter in terms of sensing sensitivity? (i.e., is thin-film structure better than the popular core-shell fiber structure?)

(3)   What is the optimum percentage of nanofillers we should use to achieve high sensitivity?

(4)   Can we achieve portable packaging for the sensing unit with desired data acquisition, processing, and transmission?

(5)   Can the artificial neural network (ANN) approach understand the relationship between strain measurements and normal load? Can it detect abnormal strain measurement?

Among them, Questions 1-3 are related to the materials and sensor fabrication, which will be addressed in Task 1. Question 4 belongs to the hardware component, which will be addressed in Task 2. Question 5 belongs to the data processing software, which will be addressed in Task 3. The specific contents of these three tasks are summarized below:

1.2.1 Task 1: Materials synthesis, sensor fabrication, and sensor validation

We will develop a low cost and efficient way to produce graphene flakes using the electrochemical exfoliation method. In addition, we will also compare the two types of sensors made with two different structures: (1) PVDF-graphene thin film sensor for small cracks; and (2) zig-zag shaped sensor with graphene coated glass fiber to cross large initial cracks. We also conducted the validation for the two types of sensors.

1.2.2 Task 2: Hardware development for data acquisition and transmission

In Task 2 we will develop the Raspberry Pi system and convert the analog signal to digital signal for the ease of data transmission and data precision. We will also develop the portable package with a solar-panel energy harvesting device for self-efficiency. In the end, we have established an online real-time database that allows us to transmit the data using a cellular network (4G) and store them in the cloud server. The cloud server is also able to message other mobile devices if certain abnormalities are observed.

1.2.3 Task 3: Software development including cloud data storage and machine learning for strain data processing

We will develop the online platform for data storage and processing. In addition, we will also explore the usage of machine learning to understand the "normal" strain variation and differentiate the abnormal signals from the normal trend. We will also validate this approach with a simple case study.

Chapter 2 Research Program

2.1 Task 1: Materials Synthesis, Sensor Fabrication, and Sensor Validation

2.1.1 Materials synthesis

The materials needed in this study are graphene flakes, PVDF polymers, PDMS polymers, and glass fibers. To reduce cost, we have developed an electrochemical exfoliation process to produce a large graphene sheet with a significantly lower cost than the conventional chemical vapor deposition (CVD) approach [10]. The specific details of material synthesis are provided below.

Graphene: In this work, electrochemically exfoliated graphene was synthesized, which has the advantage in low cost and high production. Briefly, Graphite foil (Alfa Aesar, 0.5 mm thick) was cut into 2.5 cm × 8 cm pieces and used as the anode and source of graphene for the electrochemical process, while a graphite rod (Graphite Store, diameter of 24.5 mm) was employed as the counter electrode. A 0.1 M solution of ammonium sulfate ($NaSO_4$) was purchased from Sigma-Aldrich and used as the electrolyte in aqueous solution (as shown in fig. 2.1(a)). The working electrode's exfoliation occurs as an immediate consequence of the applied voltage between the two electrodes, for example, +15 V (ISO-TECH IPS-603 DC power supply), which generates a starting current of ~0.4 A. Produced powder was collected by vacuum filtration on PTFE membranes (pore diameter of 5 μm), and after several rinsing steps needed to remove salt residuals, it was dispersed in N,N-Dimethylformamide (DMF) (Sigma Aldrich) by mild sonication for 20 min (as shown in fig. 2.1(b)). Using DMF as a solvent could help avoid the aggregation of graphene. Such dispersion was kept decanting for 48 h to promote the sedimentation of unexfoliated material. After that, a supernatant solution was taken as monolayer graphene dispersion. The lateral size of monolayer graphene is ~ 1μm. The filtration process was repeated, and the collected monolayer graphene was dried in a vacuum oven overnight for future use.

PVDF matrix materials: Polyvinylidene fluoride (PVDF) has unique properties such having the highest chemical resistance and a high temperature sustainability, and it has been applied in a wide variety of fields such as piezoelectric, pyroelectric, etc. In this work, PVDF with a molecular weight of 100000 g/mol was purchased from Alfa Aesar, and DMF was used as a solvent.

PDMS sealant materials: Polydimethylsiloxane (PDMS) Sylgard 184 was purchased from Dow Corning. The PDMS preparation procedure is as follows. Firstly, PDMS and the curing agent were mixed with a weight ratio of 10:1. Then the bubbles were removed. After pouring into the desired area, the PDMS could be cured at 70 °C for 0.5 h.

(a) Electrochemical exfoliation process   **(b)** Graphene suspension in DMF via sonication   **(c)** Stir PVDF and EG/DMF

(e) Connect electrode & spin-coating PDMS

(d)
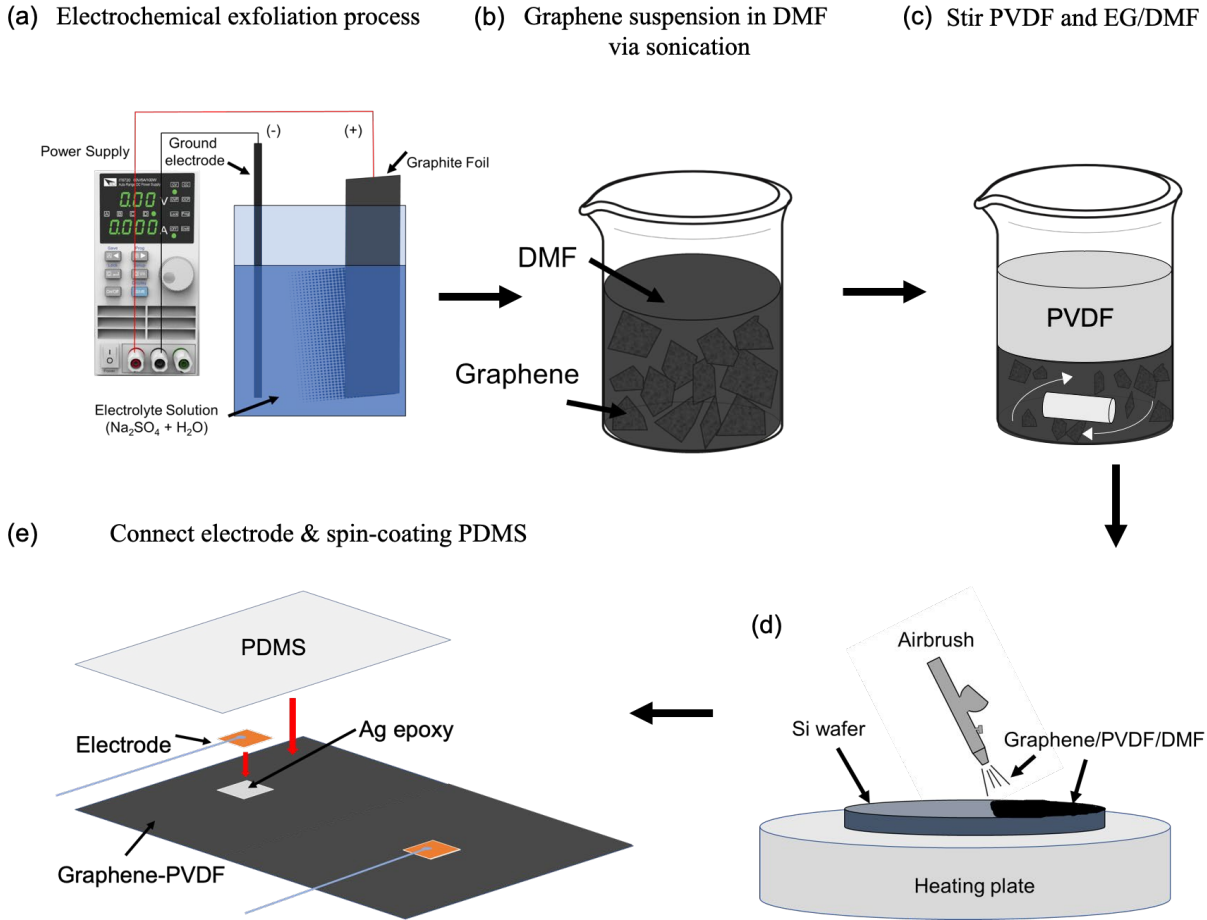
Figure 2.1 (a) Synthesize electrochemically exfoliated graphene, (b) disperse graphene in DMF, (c) mix PVDF and graphene in DMF, (d) spray PVDF/graphene to Si wafer and (e) connect wires and coat PDMS protection layer.

2.1.2 Sensor Fabrication

Two types of sensors were fabricated including the PVDF/graphene thin film sensor for the small cracks and the graphene coated fiber sensor for large cracks. For the PVDF/graphene thin film sensor, graphene was mixed with PVDF to form a thin layer with embedded electrodes. Then it was packaged with a PDMS sealant layer. For the fiber sensor, the graphene was firstly coated on top of glass fiber, then bundled and glued to the surface for crack detection. The fabrication details are described below.

PVDF/graphene thin film sensor for small cracks: To prepare PVDF/graphene nanocomposites with different weight fractions of graphene, the procedure is as follows. Initially, a fixed amount of graphene was dispersed in DMF by sonicating for 60 min. Meanwhile, a fixed amount of PVDF polymer was dissolved in DMF with the help of a magnetic stirrer for 30 min. Then, these two solutions were mixed by sonicating for 1 h, followed by magnetic stirring (as shown in fig. 2.1(c)). The mixed solution was sprayed onto a silicon wafer using an airbrush (Master Airbrush) as shown in Figure 2.1(d). The nozzle size was 0.5 mm, and the operating pressure is 80 psi. To increase the hydrophilicity of the silicon wafer surface, firstly, the silicon was cleaned by soaking in acetone at 55 °C, followed by rinsing in methanol and distilled water; then, the siliconwafer was soaked in piranha solution (vol. ratio 3:1 of H_2SO_4 and H_2O_2) for 6 h. After slowly evaporating the DMF solvent at 50 °C, a PVDF/graphene film was peeled from the siliconwafer and cut into the needed shape using a cutting machine (Silhouettes). Copper wires were bonded to the two sides of the PVDF/graphene film using a silver paste, which could greatly reduce contact resistance. At last, PDMS, which acted as a protection layer, was spin-coated onto the two sides of the PVDF/graphene film (2000 rpm for 30 s) and cured (as shown in fig. 2.1(e)).

Fiber based zig-zag sensor for large cracks: To coat the glass fibers with electrochemically exfoliated graphene, firstly, 10 mL of aqueous graphene solution (3–5 mg/mL) was poured into a plastic weighing boat (10 cm diameter). To improve the adhesion between graphene glass fibers, fiber surfaces were chemically treated and exposed to oxygen plasma. At first, glass fibers were heat treated at 600 °C for 1 h in a box furnace (Thermal Scientific) to remove residual coating on fibers from the commercial manufacturing process. Next, fibers were treated in Piranha solution for 10 min followed by washing with DI water to make the surface more hydrophilic. To coat the glass fibers with electrochemically exfoliated graphene, firstly, 10 mL of

12

aqueous graphene solution (3–5 mg/mL) was poured into a plastic weighing boat (10 cm diameter). After that, surface treated glass fiber bundles were dipped into a graphene in DMF dispersion, which contains monolayer graphene, for 5 min followed by drying in air for 5 min (as shown in fig. 2.2(a)). This process was repeated with varying number of dips from 5 to 20 and 50. The glass fiber with graphene coating is shown in Figure 2.2(b). This dip-coating method has the advantage of coating many fibers simultaneously.

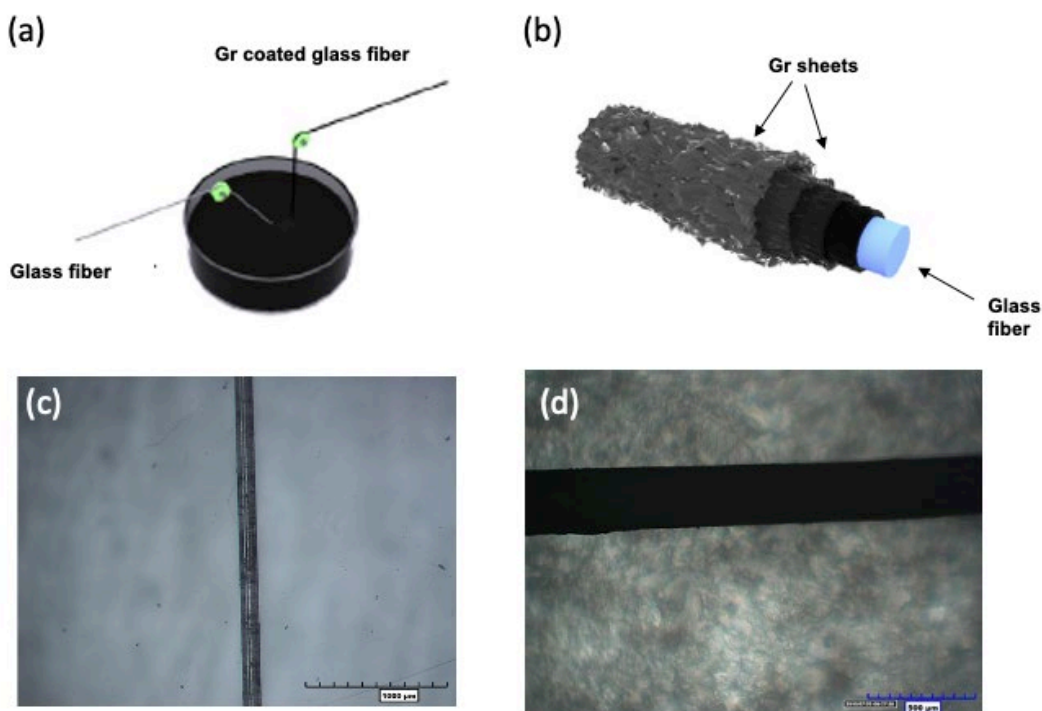Figure 2.2 (a) Coat graphene onto glass fiber surfaces, (b) the graphene coated glass fiber structure, (c) optical image of single glass fiber coated with graphene, (d) bundle of coated glass fiber.

2.1.3 Sensor Validation

Two variables were noticed to affect the film resistance during the manufacturing process of the PVDF/graphene composite: graphene concentration by weight and the stirring time of the

13

PVDF/graphene mixture. Experiment set up as shown in Figure 2.3(a) was used to study how these two factors influence the film resistance. Multiple PVDF/graphene composites with graphene concentration weights ranging from 1% to 9% were prepared and the resistance of each film was recorded as shown in Figure 2.3(b). It was found that with the increase of graphene concentration, the film resistance decreased. However, the decreasing resistance terminated at 50 kΩ when the graphene concentration arrived at 6%, which indicated the effect of graphene on increasing conductivity is saturated. The graphene with 7% concentration was used to determine the effect of stirring time of PVDF/graphene inside DMF on film resistance. Solutions were stirred from 1 to 25 hours at 2500 rpm using a magnetic stirring stick.
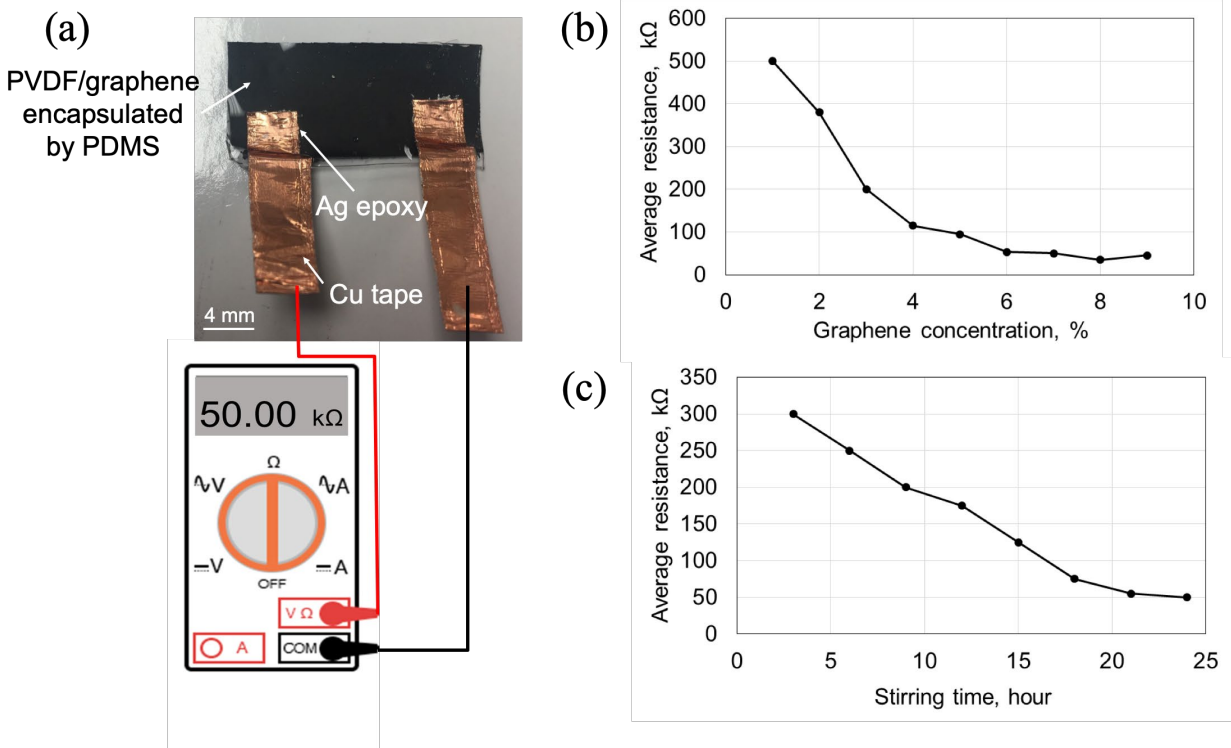

Figure 2.3 (a) Experiment set up for resistance measurements, (b) average resistance versus graphene concentration, (b) average resistance versus stirring time.

To calibrate the PVDF/graphene composite used as a strain sensor, the composite was bonded onto an aluminum plate with a pre-crack in the middle. Then the aluminum plate was loaded into Instron for tensile testing as shown in Figure 2.4(a) a load versus displacement curve could be obtained from Instron and load versus strain at PVDF/graphene bonded area could be calculated. At the same time, the resistance values of the PVDF/graphene composite were also recorded by a National Instruments Data Acquisition system with the composite in a quarter Wheatstone bridge configuration. The results were shown in Figure 2.4(b) and the gauge factor was calculated to be 20 using the equation $\frac{\Delta R/R_0}{\varepsilon}$, where ΔR is resistance change, R_0 is initial resistance, and ε is strain. Then, in the application, the strain could be calculated when the $\Delta R/R_0$ is measured.
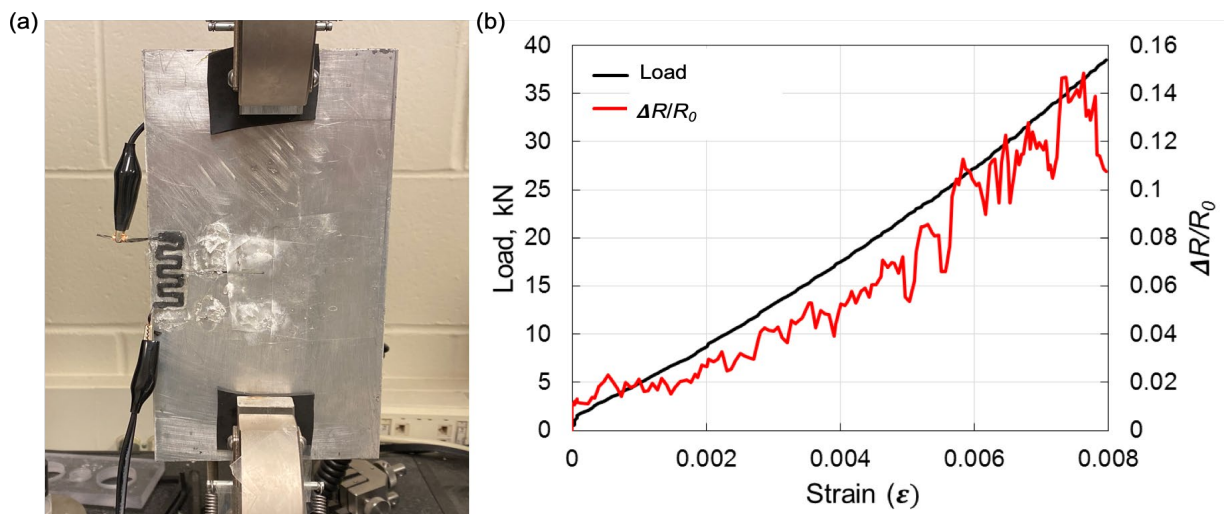

Figure 2.4 (a) Experiment set up for strain sensor calibration, (b) load versus strain and $\Delta R/R\_0$ versus strain.

Due to the limitation of glass fiber length and resolution of strain measured, a micro tensile tester was used to calibrate the graphene coated glass fiber. Copper films were glued to the edges

of the glass fiber to avoid slip between clamps of the micro tensile tester and glass fibers. Similarly, force versus strain and $\Delta R/R_0$ versus strain curves were obtained and are shown in Figure 2.5. The gauge factor was calculated to be five, which indicates the graphene coated glass fiber had less sensitivity than the PVDF/graphene composited when used as a strain sensor.
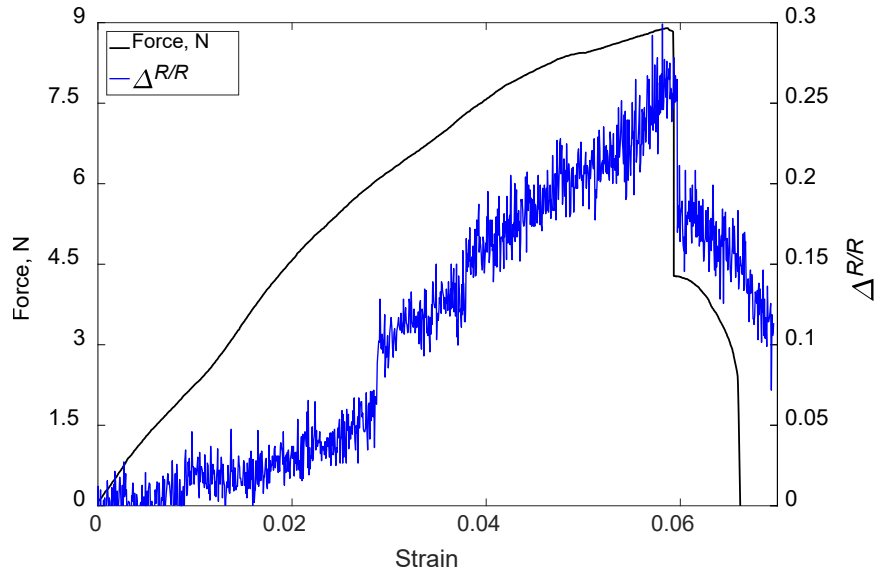
Figure 2.5 Force versus strain and $\Delta R/R\_0$ versus strain.

From the sensor validation experiments conducted, it was concluded the sensor can provide high sensitivity in terms of straining. The limit of detection for the strain was found to be about 1×10^{-4}, which is comparable to the commercially available metal coil type strain gauge. However, the range of measurements (total stretching of the sensor) is about 200% of its original length, far exceeding any commercially available metal coil type strain gauge. These results demonstrated that the developed nanocomposite sensor can satisfy the required strain measurements.

2.2 Task 2: Hardware for Data Acquisition and Transmission

2.2.1 Arduino and Raspberry Pi

In this subtask, we will compare the two data acquisition systems explored at the beginning of the research: (1) the Arduino DAQ system, and (2) the Raspberry Pi system. We utilized the Arduino DAQ system first since it was readily available in the lab and exhibited excellent performances for some of our other sensors [11]. In addition, we prefer its on-board Bluetooth transmitter, which can help us pass the data directly to our mobile computing devices. The layout of the Arduino system utilized in the calibration of our prototype sensors is shown in the Fig. 10 below.
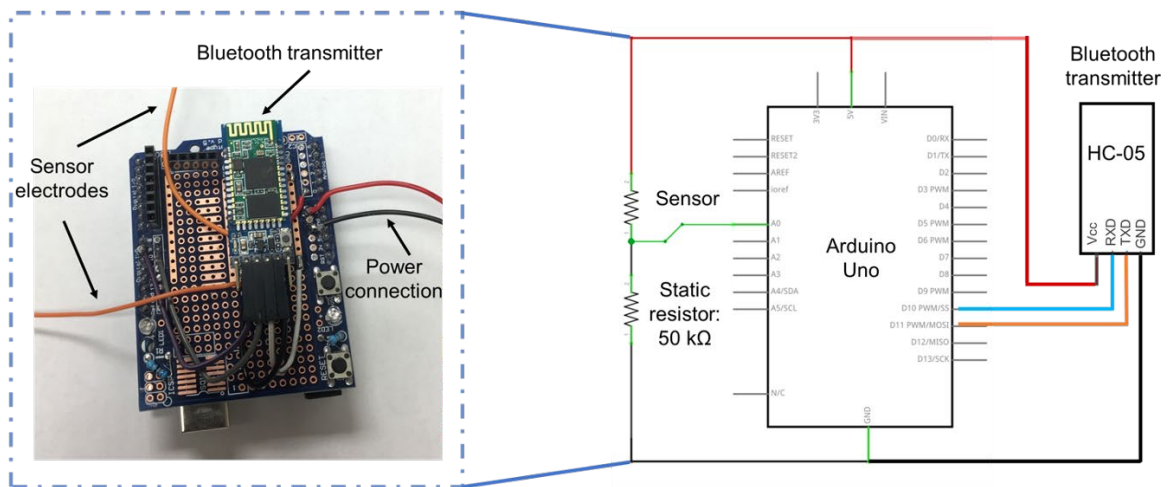
Figure 2.6 Arduino DAQ system built and utilized for our prototype sensor calibration.

In the Arduino DAQ system, the crack/strain sensor works as a potentiometer in the system where their changing resistance is measured against a constant resistance. However, we soon realized that there are several disadvantages using the Arduino DAQ system: (1) the signal output is 10-bit resolution, which gives steps of 4.88 mV, which is too coarse for fine strain readings; and (2) the Arduino DAQ system needs separation components that work with it to achieve other

functions including data transmission via cellular network, solar power management system, video recording capability, and analog to digital conversion.

Based on these limitations, we opted for the Raspberry Pi system (Pi system for short).The Pi system has four key features that allow us to take advantage of its flexibility: (1) data transmission via 4G cellular network, (2) solar power management system, (3) video feed, and (4) 16-bit resolution analog to digital conversion.

The data transmission allows the data to be transmitted in long ranges to remote servers. This also allows the server to directly receive .txt files and store them, accelerating data processing and message sending.

The solar power management system can be used to manage the power consumption to achieve long-term monitoring reliability, which is crucial to this study. For instance, with the Pi system, we have successfully demonstrated that we can utilize a 9 V battery maintained by a 6W solar panel for continuous power supply. The specific power management strategies we have explored are a (i) dynamic control of sampling rate, and (ii) periodically shutting-down and activating the system.

The Pi system allows video feed, which allows future surveillance and inspection of infrastructure. In addition, we have explored the usage of a five Megapixel camera, and up to 1080p at 36fps with a 20-180° field of view. However, due to the limitation of the scope, we did not include the details of video feed in this research.

Finally, the Pi system also has a convenient 16-bit resolution analog to digital conversion as illustrated in Figure 2.7(a). With this digital conversion, we could obtain a more precise strain data collection.

2.2.2 Standalone system

Specifically, we show the Pi-integrated sensing system (only sensor and DAC) is highly portable and can be enlosed within a water-proof box with a 9 V battery inserted as illustrated in Figure 2.8. It should be noted that each DAC system can handle eight sensors sensing and recording simultaneously. To extend the field life of the sensing system, we also equipped it with a solar power system and a charge regulator as illustrated in Figure 2.9. This solar powered system was finalized and recommended for field implementation.
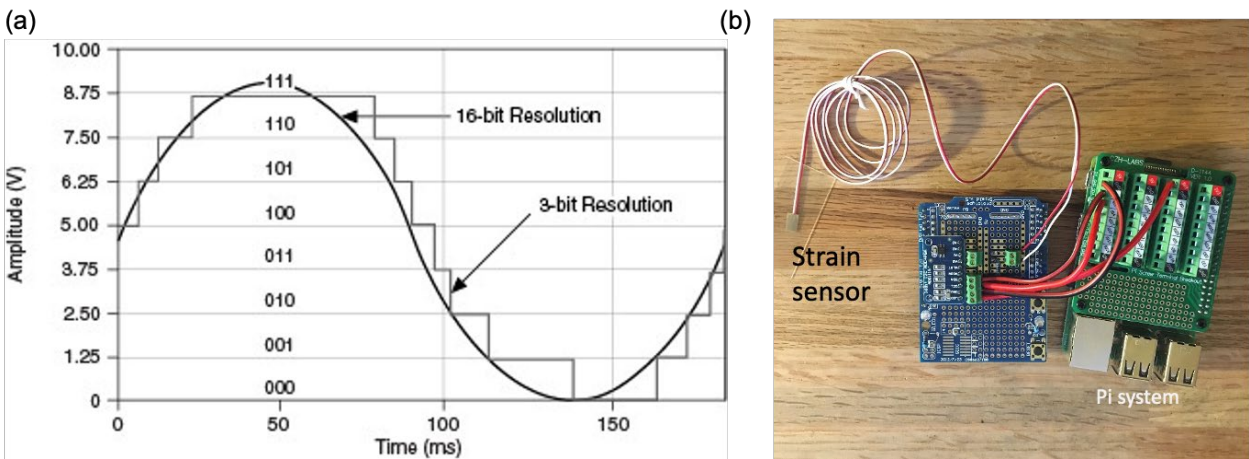

Figure 2.7 (a) Illustrative comparison of 16-bit and 3-bit resolution, (b) sensor with Pi system
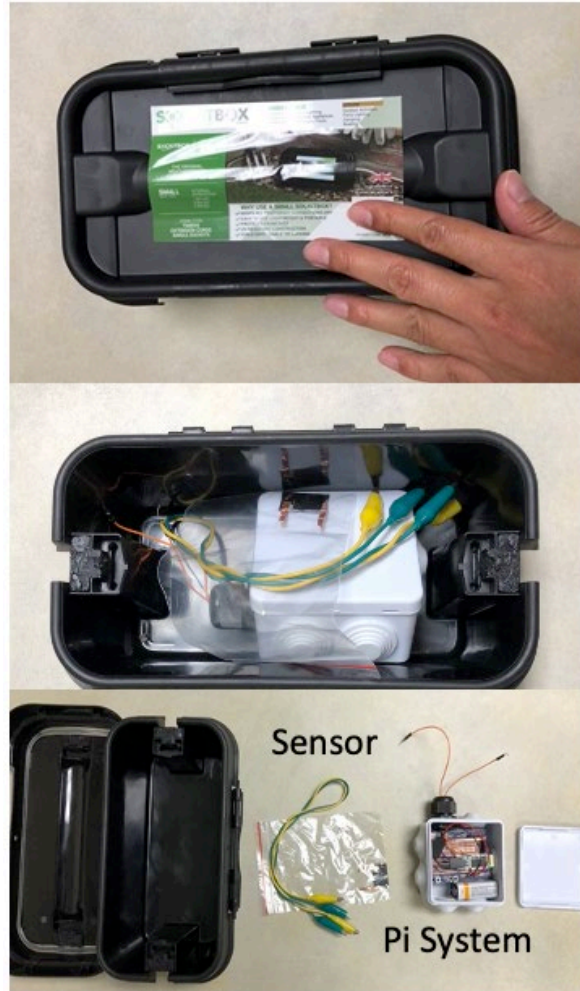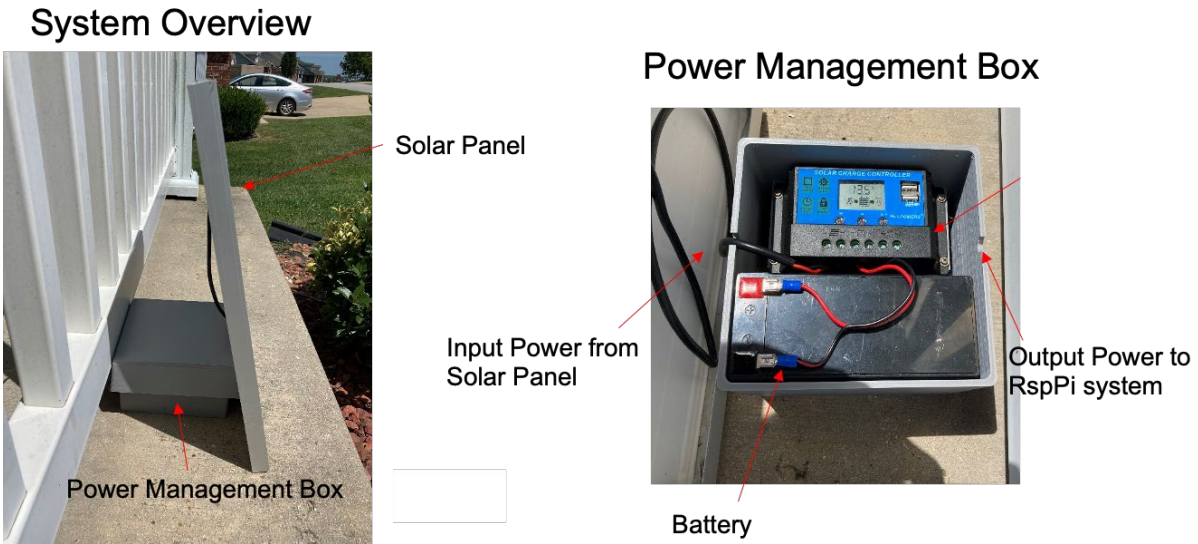
Figure 2.8 Potable sensing system

Figure 2.9 Sensing system with solar power integrated

2.3 Task 3: Software Development Including Cloud Data Storage and Machine Learning

2.3.1 Data transmission and cloud storage

With the hardware completed, we then start to build the cloud data storage, transmission mechanism as well as the machine learning assisted data processing algorithm. The data collected from the Pi-system is uploaded to the cloud through the cellular 4G network. The team has made inquiries to the local wireless communications service providers (ATT and T-mobile). The cost of each data transmission line is about $15-$25 (no images), which is sufficient for more than 100 sensors if data management is implemented (dynamic scanning rate). For the server, we utilize the free online service from Google Firebase Realtime Database [12].

The preliminary data transmitted to the server using the temporary sim card are plotted in Figure 2.10. It should be noted that the web app was programmed to display these data in real-time, which can also be sent to cellphones or other mobile computing devices.

Figure 2.10 (Top panel) Sensing data uploaded to server and displayed on web app in real-time: x-axis is time in hour, y-axis is the resistance readings in ohm; (bottom panel) cloud data service by firebase.

For the preliminary test, the strain/crack sensors were attached to the railing of the residential building as illustrated in Figure 2.11. From the sparse data displayed in Figure 2.10 (which is adjustable by using different scanning rate), we have found that the strain data fluctuates significantly with respect to time. It is suspected that the sensors are sensitive to thermal fluctuation, periodic local vibration, as well as other disturbances. These complex environmental loadings, especially the thermal effect, should be excluded when judging the abnormal strain increase due to excessive structural load.
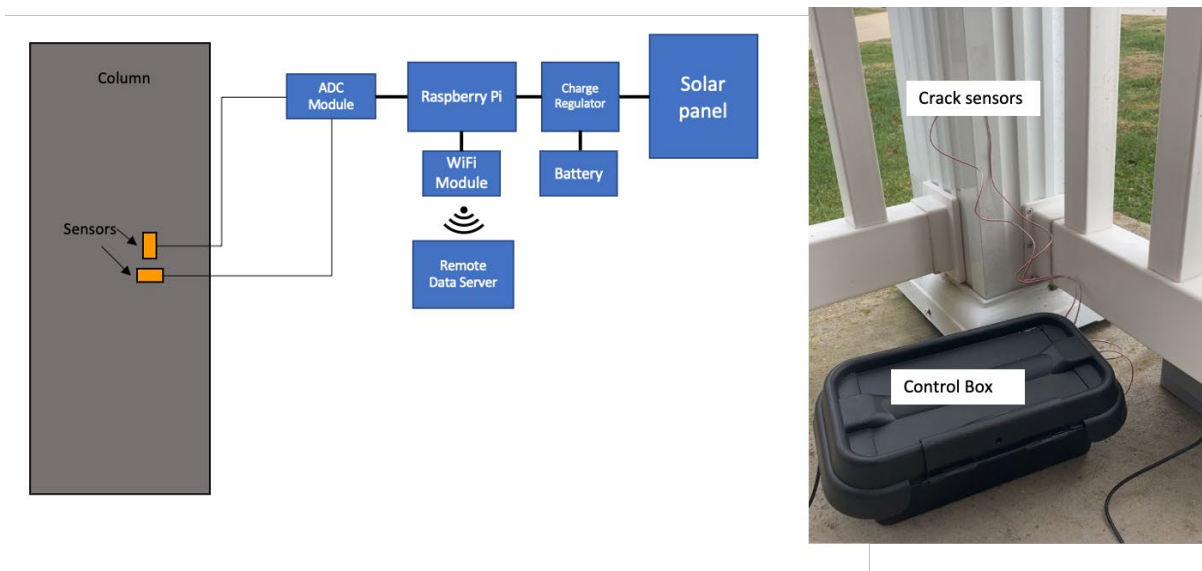
Figure 2.11 (Left panel) illustration of sensing system, (right panel) sensor installation location with control box nearby.

2.3.2 Machine learning understanding thermal straining and abnormal signal detection

Thermal strain is a critical aspect in structural engineering. Several researches have been conducted in correlating temperature with the strain reading. However, most of these works focus on eliminating thermal expansion of the sensor, i.e., strain gauges themselves. Very few works have been conducted to understand the effect of temperature on structural loading and response. Yet, a tremendous number of structural failures can be directly related to thermal cycling. Perhaps, the actual reason behind this scarcely investigated issue is its complexity in nature. The coupling between the change of boundary conditions and thermal cycles, which is the cause of the structural loading caused by thermocycling, is almost impossible to decipher. In this work, we will utilize a deep learning neural network model to extract this coupled relation and use it in an analytical model to predict the behavior of the structures using only experimental data. This experimental data will come from active monitoring systems measuring thermal strain on members over time.

23

Using these systems with deep learning methods would allow us to determine the structural conditions of infrastructure more accurately.

Strain data was collected from an aluminum support column for a railing assembly and awning. Two sets of strain gauges were placed on the column on opposite sides to classify the type of stress the column is under (tension, compression, or combination). The strain gauges in each set are installed perpendicular to each other to collect a strain value in both the x and z direction. Strain data was collected from the gauges using a Raspberry Pi 3 B+ with a 16-bit analog to digital (ADC) board which allows the Pi to understand the analog signals. The testing setup and DAQ system is presented in Figure 2.11. Data was collected each hour measuring 10 strain data points and the current temperature. All the data was backed up to a database in Google Firebase. The strain data points for each temperature were averaged to produce a model of the temperature vs strain relationship. Another test was conducted in which an external strain was applied to cause a disturbance in the data.

The data from these tests was initially simulated using the 'sklearn' and 'mpl' neural network packages in Python to simulate supervised learning techniques. This method was replaced with MATLAB's neural networking toolbox as the Python program was not accurate enough with the amount of collected data points. Data fitting and prediction functions were used in the MATLAB toolbox to create data plots of input output and test point plots along with their error. Figure 2.12 presents the work schematics followed to find the desired relationship. Both the Python and MATLAB programs used in the experiment can be found in this section.
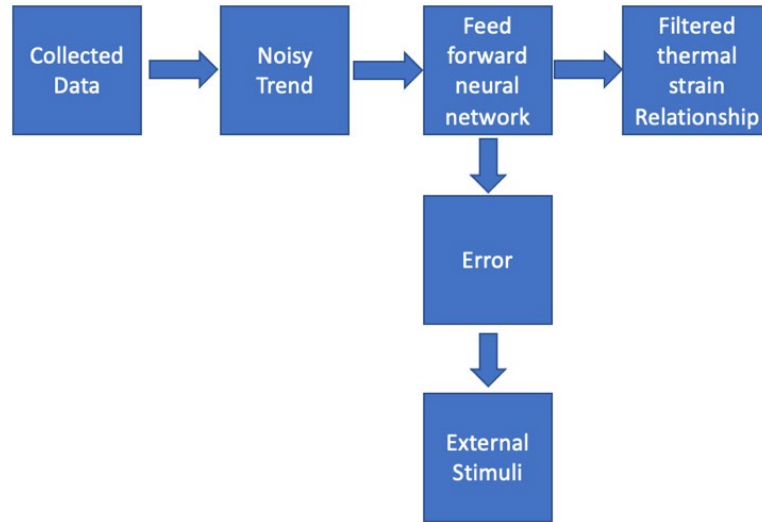
Figure 2.12 Workflow scheme followed to develop relationships

The first simulation conducted in the experiment was with a Feed Forward Neural Network with 10 hidden layers. The Levenberg-Marquardt method was used to train the network and its performance was determined through the mean squared error. The neural network and its structure can be seen in Figure 2.13. Figure 2.14 presents the structures of the neural network used with the input being temperature and the output being strain. From the fit plot in Figure 2.13, some initial error in the training targets can be seen as the fitting curve stays more linear rather than fluctuating with the input data. This behavior reflects into the test targets and outputs with errors on each point averaging approximately 1.625 ohms. Since strain gauges are highly sensitive, the goal is to lower this error as much as possible to lower than 1 ohm to ensure accurate prediction capabilities. In Figure 2.14, the networks performance of training, testing, and validating data points is presented. Using 10 hidden layers, the network had its best validation performance of 2.1628 at its 4th epoch. As shown on the plot, after 10 epochs, the validation performance does not reach an equilibrium level, indicating some fluctuations in the accuracy of the network.
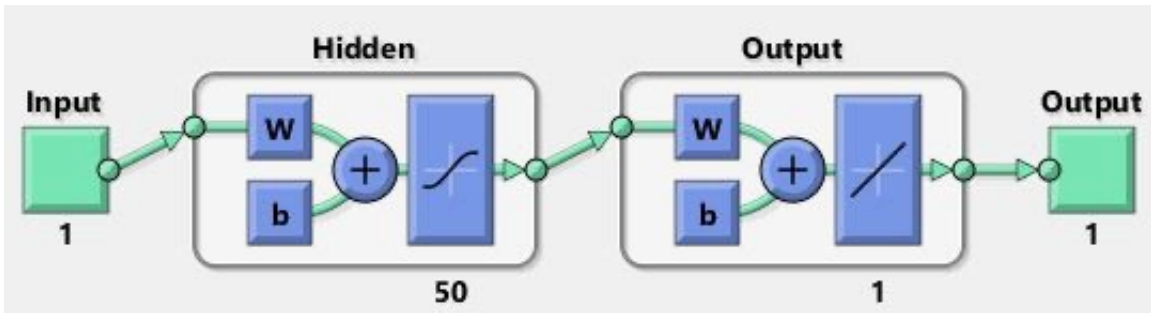
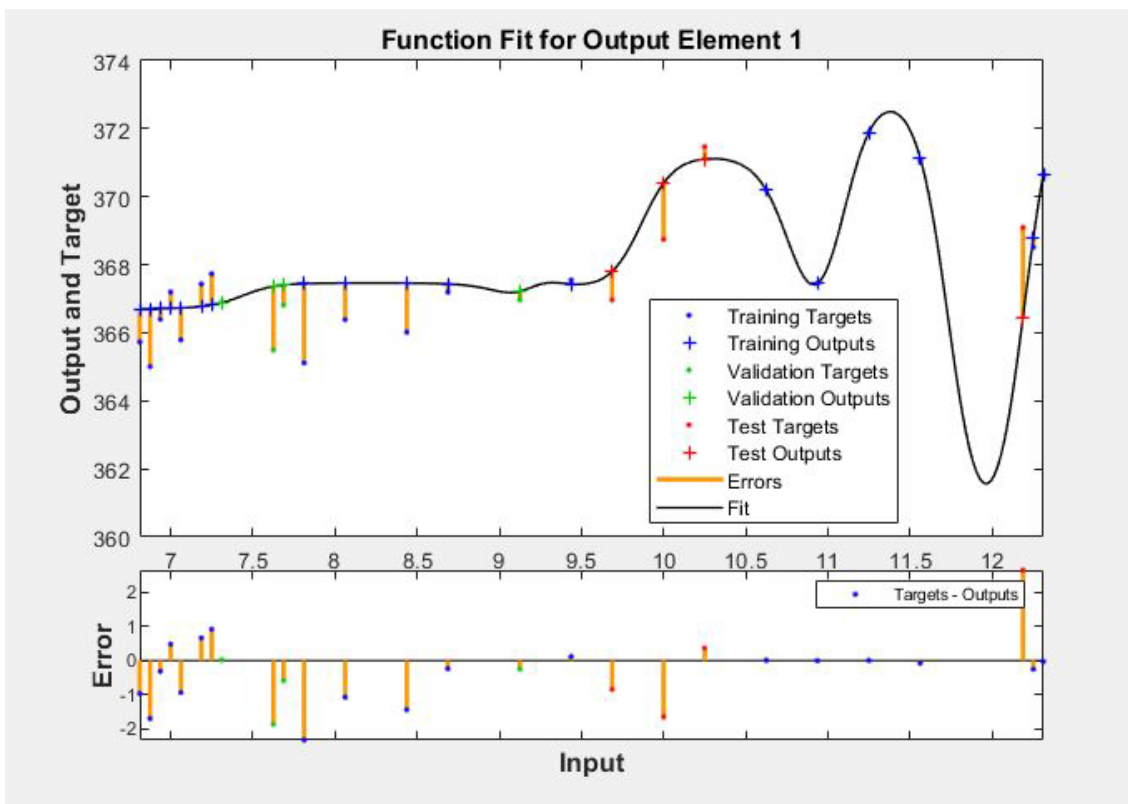Figure 2.13 Feed forward neural network structure

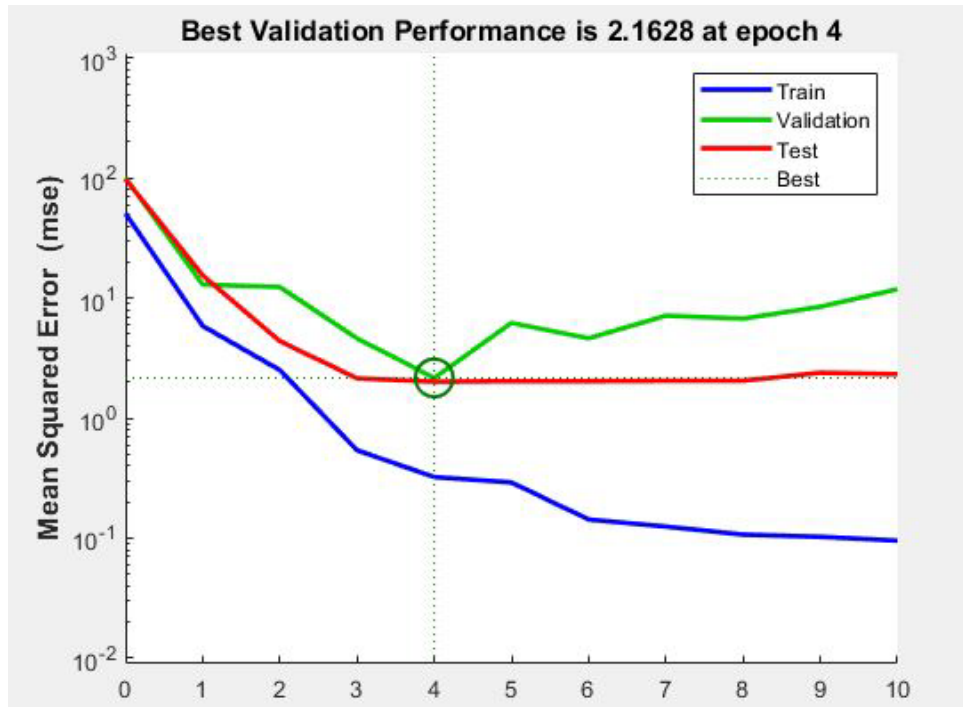Figure 2.14 System fit of network with 10 hidden layers

Figure 2.15 Performance results of network with 10 hidden layers

Further simulations were conducted for the system by increasing the number of hidden layers in the network. Figures 2.16 and 2.17 present the systems fit and performance after being simulated with 50 hidden layers in the network. Looking at the fit in Figure 2.16, the system has more fluctuations but has little to no errors regarding the training data. This behavior reflects the test data points with an average error of 0.875. Increasing the number of hidden layers allowed the system to reduce the error in training and test inputs but did see a slight increase in the validation errors when compared to the network with 10 hidden layers. The performance of this network showed a much quicker stabilization than the previous test and had a significantly larger performance of 10.4865 at its second epoch. This increase in performance can be linked to the network's increase in hidden layers and being able to process these data points through five more layers. Along with this, training, testing, and validating data points were all able to come to an

equilibrium efficiency equal to or less than one, creating stability in the prediction of data points.

This stability is important to be able to properly understand and calibrate the output of the system.
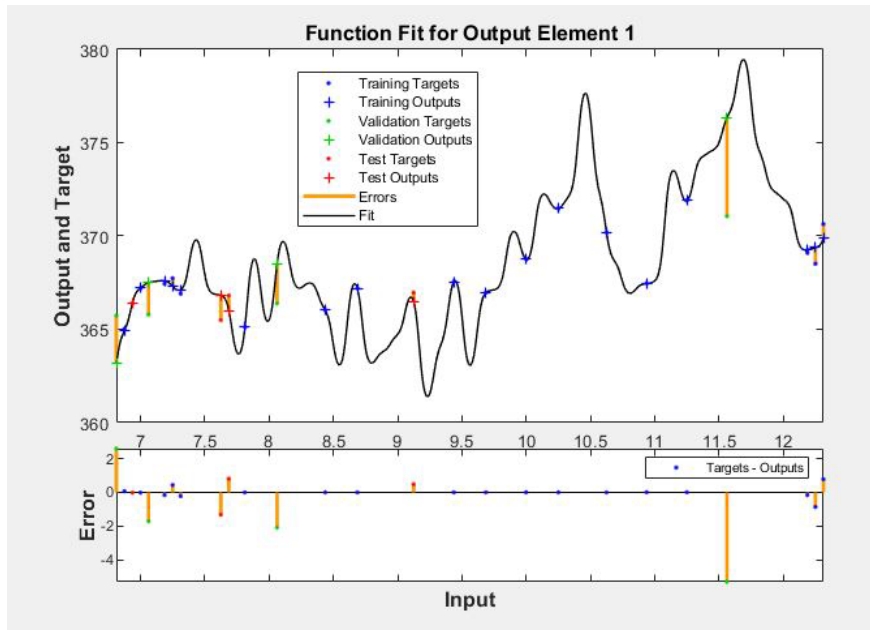

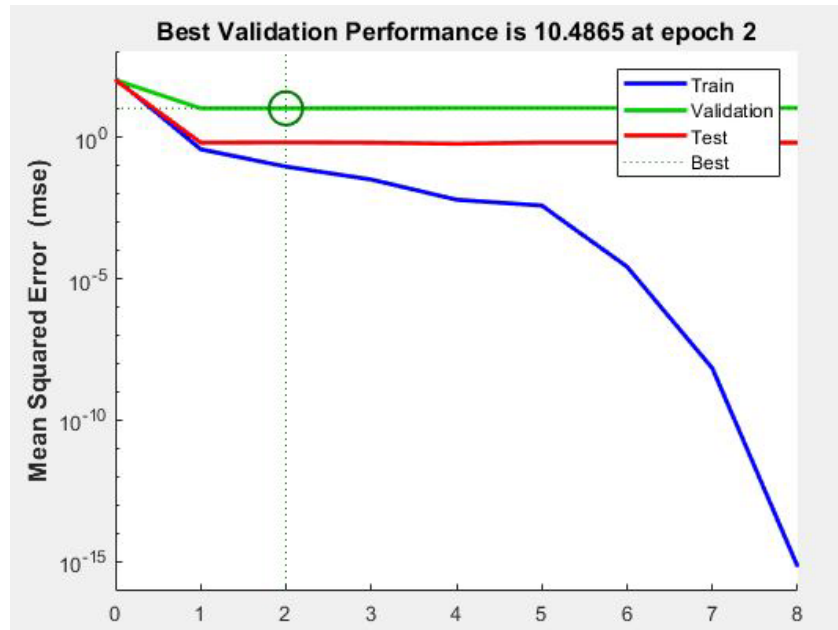Figure 2.16 System fit of network with 50 hidden layers

Figure 2.17 Performance results of network with 10 hidden layers

The final simulation was to reflect the system with disturbances included as shown in Figure 2.18. Disturbances in the system can indicate large induces loads from an external source. Data from these disturbances provide valuable information in analyzing the structural loading and condition of the members. The disturbance in the data set provides the system with a larger outlier and impacts its performance. Testing various numbers of hidden layers, a total 25 proved to create the best fit with the smallest errors. With the disturbance in the system, the network must compare the thermal strain values to the external loads. In Figure 2.18, the fit of the system with a disturbance located at 9.25 is shown. The fit line follows the training data points to develop a temperature relationship and has a large error spike at 9.25. This is due to the system expecting one value along the temperature fit and getting a much larger value from the disturbance. Having this larger outlier has impacts on the errors elsewhere in the systems predictions and stability. Although the system has a larger error, the disturbance location and how it impacts the system is crucial in being able to analyze pure thermal straining. Along with this, being able to detect disturbances in the DAQ system can provide valuable feedback to pinpoint their time and locations.

29

Using this information, a more accurate representation of the strain field on structures can be developed.
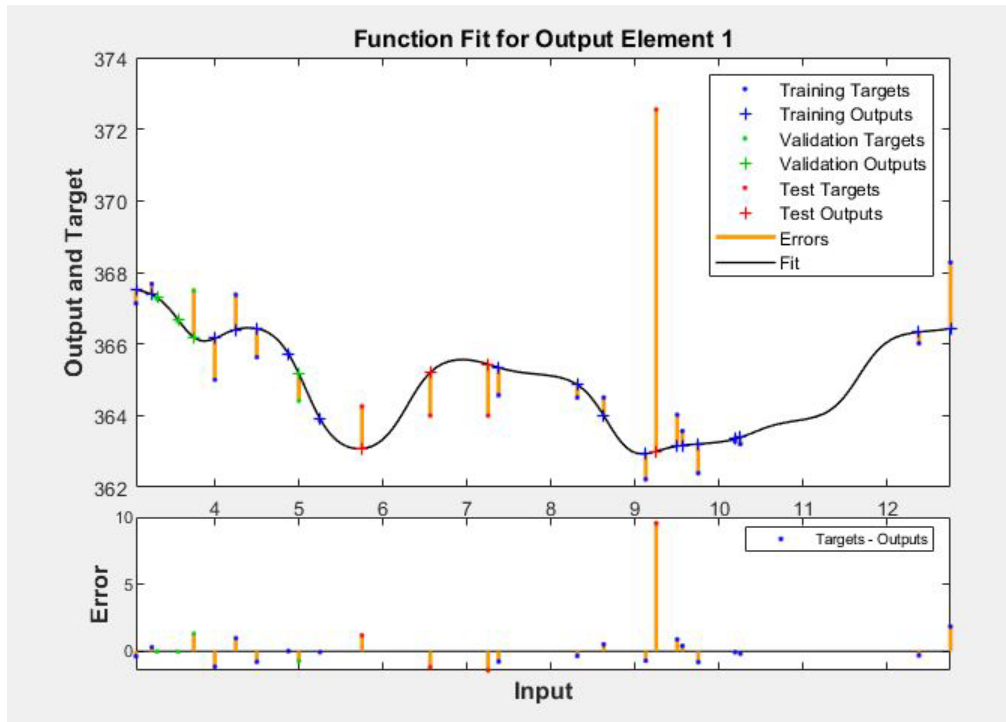

Figure 2.18 System fit of network with 25 hidden and included disturbances

Strain data was collected for different temperatures to develop a profile for thermal cycling on structural members but proved to be less stable than initially predicted due to external stimuli. A feed forward neural network was used to simulate the data collected from the test with temperature being the input and strain being the output. One simulation used a network with 10 hidden layers to develop a relationship and had an average error of 1.625. From the simulations with a network of 50 hidden layers a relationship was created with an average error of 0.875 (Ω). This showed that the neural networks performance had a strong dependency on the number of hidden layers. Another simulation was conducted with large stimuli added and the system was added followed the temperature trend with a large detected error at the spot of stimuli. This

indicates that using neural networks can be used to detect external stimuli and as a filtering effect to study thermal strain cycles. From this study, deep learning and supervised learning techniques can be used to in structural monitoring infrastructure with complex loading fields and detect abnormalities.

The Python and MATLAB codes are listed below.

Python Code

```python
# import


import numpy as np

import pandas as pd

import matplotlib

import matplotlib.pyplot as plt

from sklearn.neural_network import MLPRegressor

from sklearn.linear_model import Ridge

from mpl_toolkits.mplot3d import Axes3D

dataset=pd.read_csv('C:/users/westo/Desktop/sn1.csv')

X = dataset.drop('sn1', 1)

Y = dataset['sn1']

X1 = X['temp']

#X2 = X['delta']

# NN training function
```

```python
def model_sales_MLP(dataset, hidden, print_coefs = True, max_iter= 10000000):

    num_samples = dataset.shape[0]

    cutoff = (num_samples * 26) // 27

    Xtrn = dataset.drop('sn1', 1).iloc[:cutoff,:]

    Ytrn = dataset['sn1'].iloc[:cutoff]

    Xval = dataset.drop('sn1', 1).iloc[cutoff:,:]

    Yval = dataset['sn1'].iloc[cutoff:]

    model = MLPRegressor(hidden, validation_fraction = 0, solver='adam', max_iter=
max_iter).fit(Xtrn, Ytrn)

    coefs = model.coefs_

    yhat = model.predict(X)

    yhatval = model.predict(Xval)

    loss = np.square(Yval - yhatval).mean()

    hiddens = coefs[0].T

    final_mlp = coefs[1].flatten()

    coefs = list(zip([dict(zip(X.columns, h)) for h in hiddens],

            [['output mult:', m] for m in  final_mlp.flatten()],

            [['intercept:', i] for i in  model.intercepts_[0]]))

    print('loss:', loss)

    return model, yhat, coefs, loss
# NN learning and exporting to csv file
model, yhat, coefs, loss = model_sales_MLP(dataset, [2])
```

```python
    model, yhat, coefs, loss = model_sales_MLP(dataset, [2], max_iter = 50000000,
print_coefs=False)

    model, yhat, coefs, loss = model_sales_MLP(dataset, [2], max_iter = 50000000,
print_coefs=False)

    dataprint = pd.DataFrame({

        'yhat': yhat

    }).round(5)


    dataprint.to_csv('C:/users/westo/Desktop/sn_norm.csv')

    dataset1=pd.read_csv('C:/users/westo/Desktop/sn1-dndt.csv')

    pred = model.predict(dataset1)

    predprint = pd.DataFrame({

        'pred': pred

    }).round(5)

    predprint.to_csv('C:/users/westo/Desktop/sn_psid_norm.csv')
```

MATLAB Code

```matlab
dataset = xlsread('sn1.xlsx', 'Sn1', 'A1:B27');

x = dataset(:,1)';

t = dataset(:,2)';


% Choose a Training Function
```

```matlab
% For a list of all training functions type: help nntrain

% 'trainlm' is usually fastest.

% 'trainbr' takes longer but may be better for challenging problems.

% 'trainscg' uses less memory. Suitable in low memory situations.

trainFcn = 'trainlm';  % Levenberg-Marquardt backpropagation.


% Create a Fitting Network

hiddenLayerSize = 50;

net = fitnet(hiddenLayerSize,trainFcn);

% Setup Division of Data for Training, Validation, Testing

net.divideParam.trainRatio = 70/100;

net.divideParam.valRatio = 15/100;

net.divideParam.testRatio = 15/100;

% Train the Network

[net,tr] = train(net,x,t);


% Test the Network

y = net(x);

e = gsubtract(t,y);

performance = perform(net,t,y)


% View the Network

% view(net)
```

```matlab
% Plots

% Uncomment these lines to enable various plots.

%figure, plotperform(tr)

%figure, plottrainstate(tr)

%figure, ploterrhist(e)

%figure, plotregression(t,y)

%figure, plotfit(net,x,t)
```

Chapter 3 Results & Discussion

We would like to discuss the results from the research program by answering the critical questions raised in the introduction section.

(1)   Can we achieve low cost, large scale processing to deliver high quality of graphene needed for the sensor fabrication?

The answer is yes. The electrochemical exfoliation method developed in this study has produced good quality graphene. We have compared the Raman spectroscopy data and found the characteristic 2D and G peaks as normally observed for CVD (fig. 3.1) produced high quality monolayer graphene (fig. 3.2).
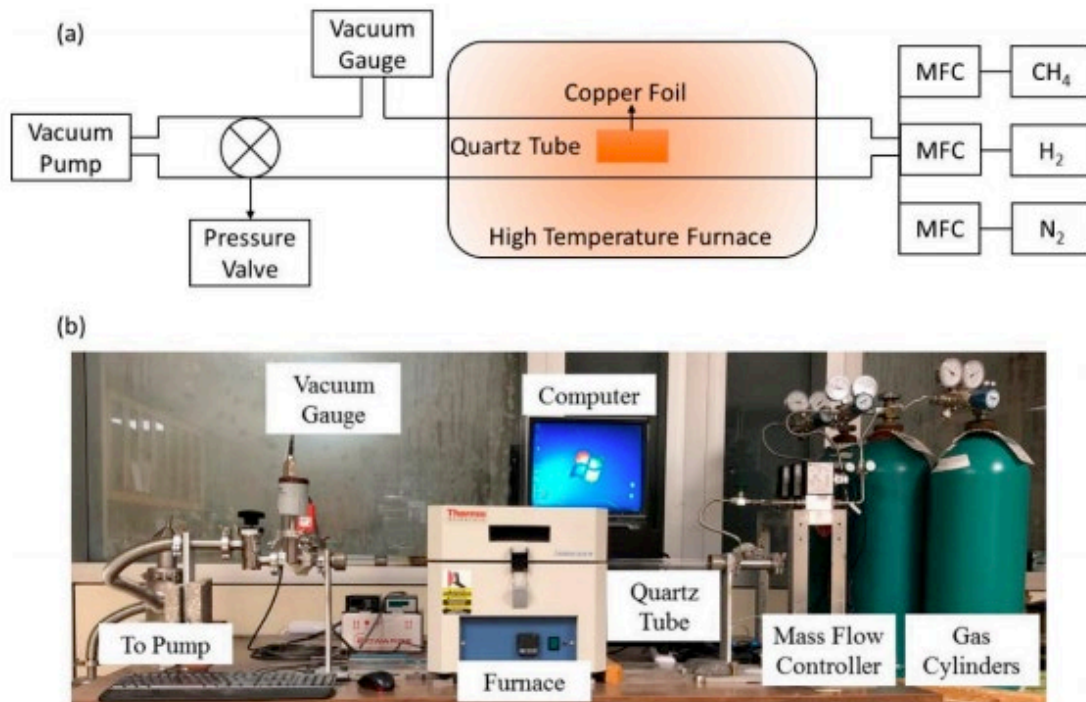

Figure 3.1 (a) Schematic illustration and (b) setup of the low-pressure chemical vapor deposition system, MFC, mass flow controller for graphene growth [13].
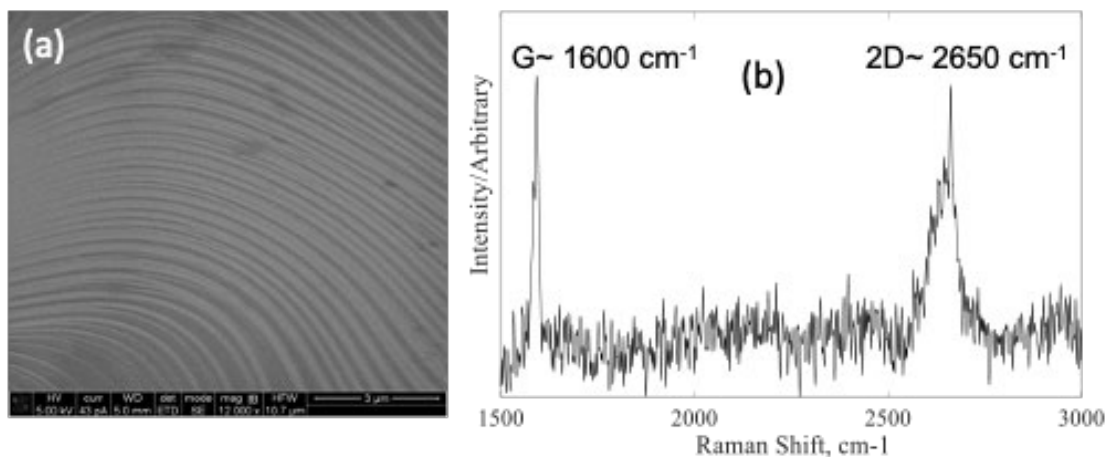
Figure 3.2 (a) Monolayer graphene on copper substrate and (b) Raman spectroscopy of monolayer graphene

These results give us high confidence of utilizing graphene to fabricate a large quantity of sensors, since the converted price for the electrochemically exfoliated graphene is below one dollar per gram. It should be noted that, one gram of graphene could be utilized in more than 10 sensors, which gives us confidence for even larger scale applications.

(2)   Does the microstructure of the sensor matter in terms of sensing sensitivity? (i.e., is thin-film structure better than the popular core-shell fiber structure?)

Both thin film and core-shell fiber sensors work very well for small and large cracks. The sensitivity is almost the same. However, for the glass fiber sensor, the measurements range varies depending on the zig-zag shape and the number of fibers in the bundle. By allowing the fibers to slip onto each other, we could achieve a longer range of measurements. By increasing the number of folds in the zig-zag pattern, we could also increase the range of measurements. However, the durability of the fiber sensor is still a question. Under environmental exposure, the loosely coated graphene flakes could be debonded from the fiber due to thermal strain and abrasion at sensor-

object interface. Therefore, additional researches are needed to evaluate the durability of the sensors.

(3)   What is the optimum percentage of nanofillers we should use to achieve high sensitivity?

Approximately 8% concentration was found to be the best filling ratio. When exceeding this value, we have found that the electro-resistance of the PVDF/graphene thin film does not significantly change, which indices excessive contacts have been established within the graphene network structure. Beyond this threshold, a nonlinear relationship is expected between the sensor straining and resistance change.

(4)   Can we achieve portable packaging for the sensing unit with desired data acquisition, processing, and transmission?

Yes. We have successfully integrated the sensor with the compact Pi-system and a 9 V battery that can collect, process, and transmit data to the cloud server using a cellular (4G) network. The entire system can fit into a palm size waterproof box. To allow continuous monitoring, we also equipped the system with a solar panel and charge it regularly, which can be stationed nearby the bridge sites. One station can safely handle more than 100 sensors provided a dynamic scanning rate is allowed to minimize energy consumption.

(5)   Can an artificial neural network (ANN) approach understand the relationship between strain measurements and normal load? Can it detect abnormal strain measurement?

Yes, but not completely. The current results showed that the supervised neural network can learn the thermal strain fluctuations coming from the real-world experiment. It also detects sudden change from strain reading due to disturbances. However, this was done with data collected in the relatively short amount of time and with the human understanding that thermal straining is the

main reason for data fluctuation. To teach machine learning the complex loading, more field experiments are needed.

Chapter 4 Conclusions & Future Studies

This pilot study on developing a wireless crack sensing system for bridges has successfully delivered the targeted sensing system with all functions including sensing, data processing, transmission, data interpretation, and abnormality detection. This system was achieved by integrating materials science (specifically nanomaterials), electrical engineering (specifically hardware on data acquisition and computer communication, power management), as well as computer science (specifically machine learning). The success of this project showed that current engineering solutions need a highly inter-disciplinary and convergence research, which does not only require the seamless integration of available engineering tools, but also novel development in all fields. Specifically, we developed new material synthesis approaches, a new sensor fabrication process, new data acquisition approaches, and new data interpretation methods. With all these developments, we have showcased the practical application of a wireless crack sensing system for the department of transportation.

However, a few issues remain to be addressed. Due to the impact of COVID-19, the field implementation was compromised, which could reveal practice problems when installing and operating the developed system at the bridge sites. Other potential issues include the durability of the bond between the sensor and the cracking surface, the reliability of the data transmission in rural areas with unstable cellular networks, and the battery maintenance for long term monitoring. These issues will be better solved in future field experiments.

In terms of outputs, this research has produced two journal publications, which are in preparation, and two poster presentations in international conferences. The funding support from this project supported one Ph.D. student and one Master's student. The prototype sensors and data systems are ready to be transferred to the Missouri Department of Transportation through seminars and formatted documents and drawings.

References

1. NACE, *Corrosion Costs and Preventive Strategies in the United States*. National Technical Information Service, 5285 Port Royal Road, Springfield, VA 22161.

2. Editorial. *HBM Strain Gauges: The First Choice for Your Strain Measurement*. [cited 2021; Available from: https://www.hbm.com/en/0014/strain-gauges/.

3. Editorial. *Strain Gauge - Part 1*. 2009 2021]; Available from: https://engineers4world.blogspot.com/2009/10/stain-gague-part-1.html.

4. Yin, Zhaozheng, Chenglin Wu, and Genda Chen, *Concrete crack detection through full-field displacement and curvature measurements by visual mark tracking: A proof-of-concept study.* Structural Health Monitoring, 2014. **13**(2): p. 205-218.

5. Kharroub, Sari, Simon Laflamme, Chunhui Song, Daji Qiao, Brent Phares, and Jian Li, *Smart sensing skin for detection and localization of fatigue cracks.* Smart Materials and Structures, 2015. **24**(6): p. 065004.

6. Huang, Haizhou, Shi Su, Nan Wu, Hao Wan, Shu Wan, Hengchang Bi, and Litao Sun, *Graphene-based sensors for human health monitoring.* Frontiers in chemistry, 2019. **7**: p. 399.

7. Puértolas, JA, JF García-García, F Javier Pascual, José Miguel González-Domínguez, MT Martínez, and Alejandro Ansón-Casaos, *Dielectric behavior and electrical conductivity of PVDF filled with functionalized single-walled carbon nanotubes.* Composites Science and Technology, 2017. **152**: p. 263-274.

8. Maity, Nirmal, Amit Mandal, and Arun K Nandi, *Interface engineering of ionic liquid integrated graphene in poly (vinylidene fluoride) matrix yielding magnificent improvement in mechanical, electrical and dielectric properties.* Polymer, 2015. **65**: p. 154-167.

9. Editorial. *Teach, Learn, and Make with Raspberry Pi*. [cited 2021; Available from: https://www.raspberrypi.org/.

10. Li, Yanxiao, Shuohan Huang, Congjie Wei, Chenglin Wu, and Vadym N Mochalin, *Adhesion of two-dimensional titanium carbides (MXenes) and graphene to silicon.* Nature communications, 2019. **10**(1): p. 3014.

11. Chen, Shikun, Yanxiao Li, Dongming Yan, Chenglin Wu, and Nicholas Leventis, *Piezoresistive geopolymer enabled by crack-surface coating.* Materials Letters, 2019. **255**: p. 126582.

12. Editorial. *Firebase Realtime Database*. 2021 [cited 2021; Available from: https://firebase.google.com/docs/database.

13.   Guo, Chuanrui, Yanxiao Li, Yanping Zhu, Chenglin Wu, and Genda Chen, *Synthesis and Characterization of Free-Stand Graphene/Silver Nanowire/Graphene Nano Composite as Transparent Conductive Film with Enhanced Stiffness.* Applied Sciences, 2020. **10**(14): p. 4802.

Appendix A Additional Information

This appendix contains additional figures for the sensor fabrication.
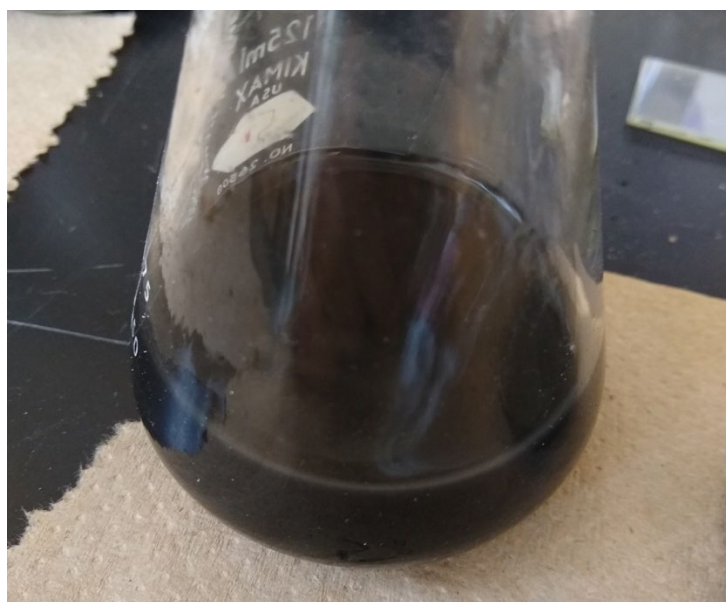

Figure A.1 Airbrush used to apply coating
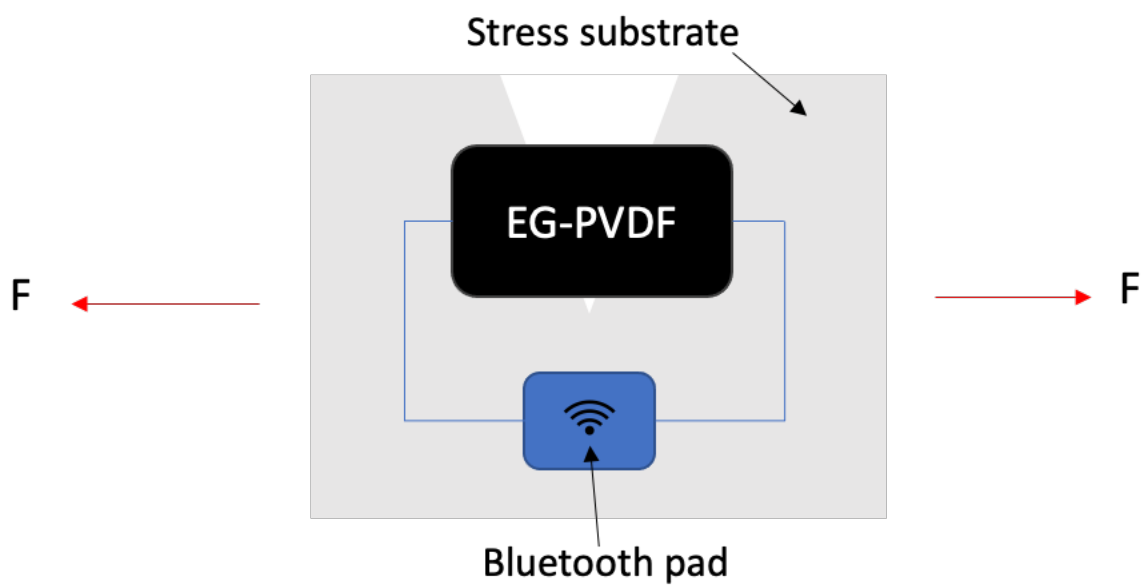

Figure A.2 8% PVDF/graphene suspension

Figure A.3 Alternative flexible sensing system design (unexplored)
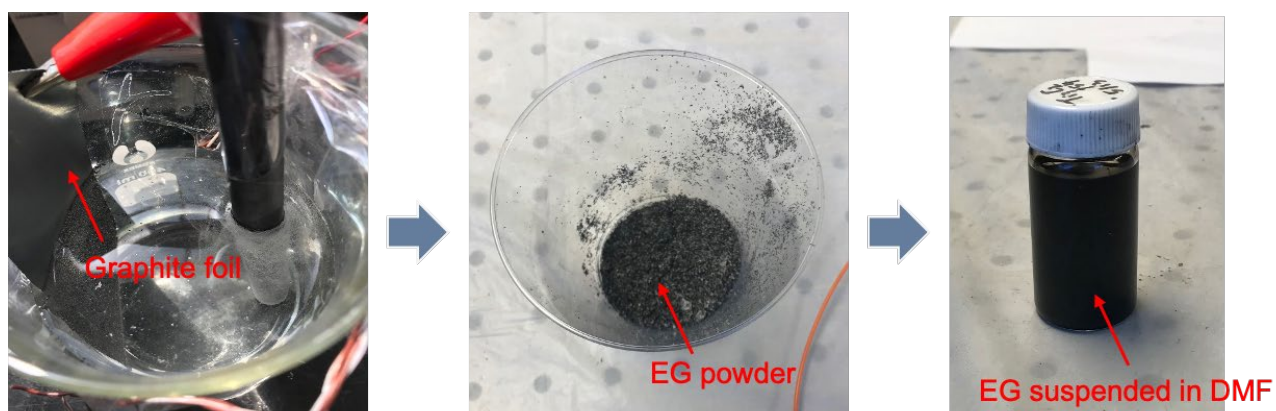
Figure A.4 Electrochemical exfoliation of graphene process
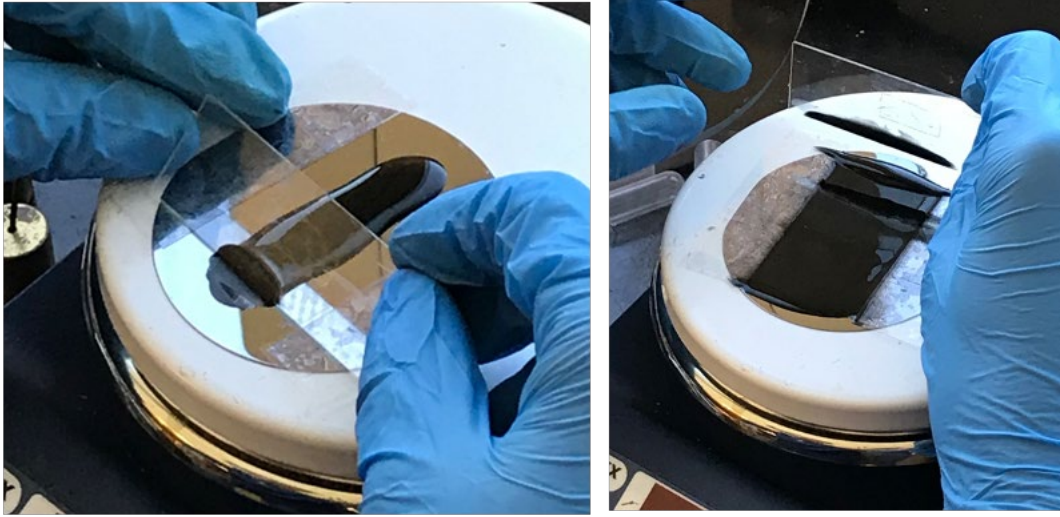
Figure A.5 Preparing PVDF/graphene paste
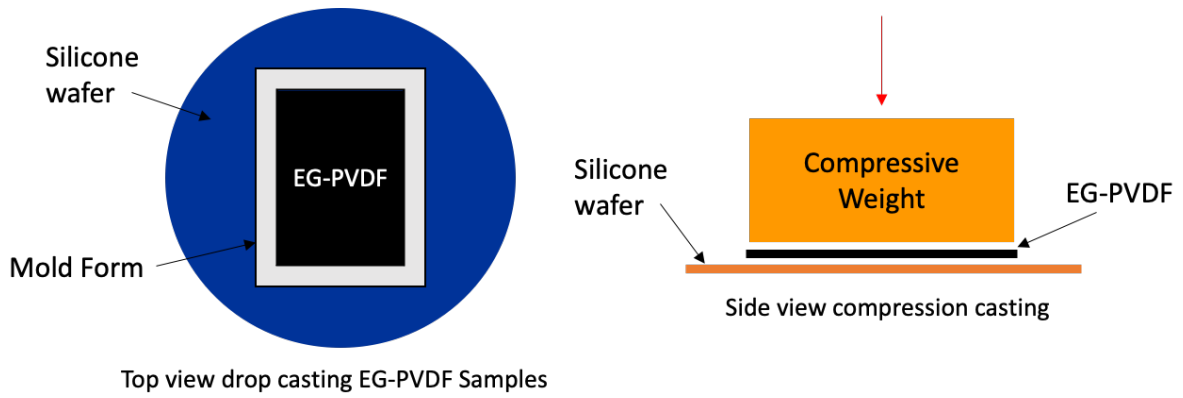
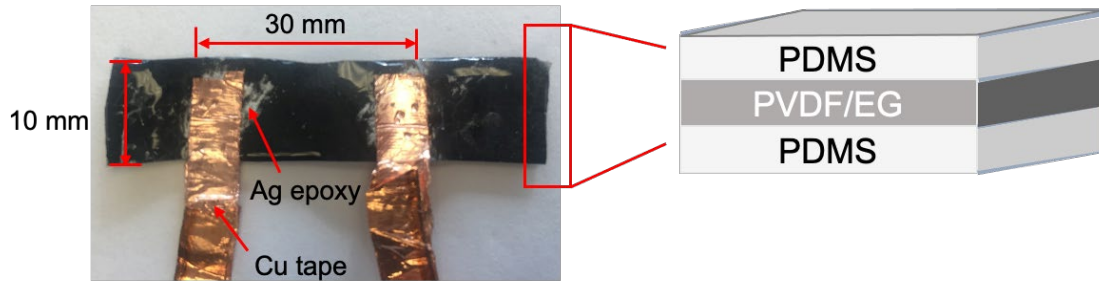Figure A.6 Preparing PVDF/graphene paste: weighted curing

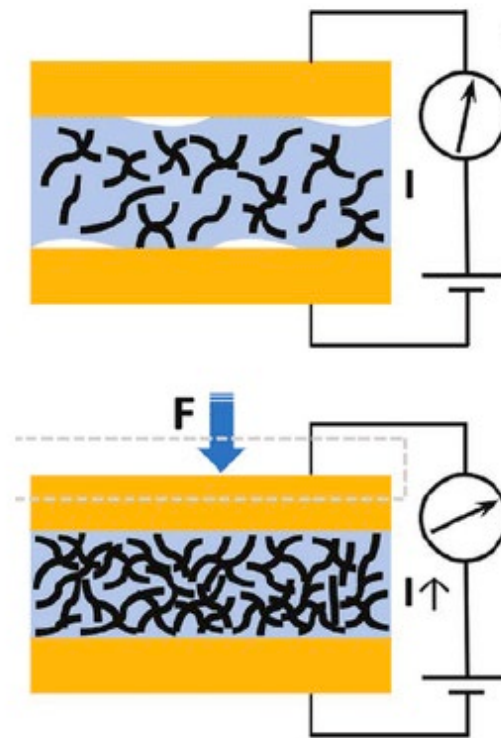Figure A.7 Dimension and structure of the thin film sensor

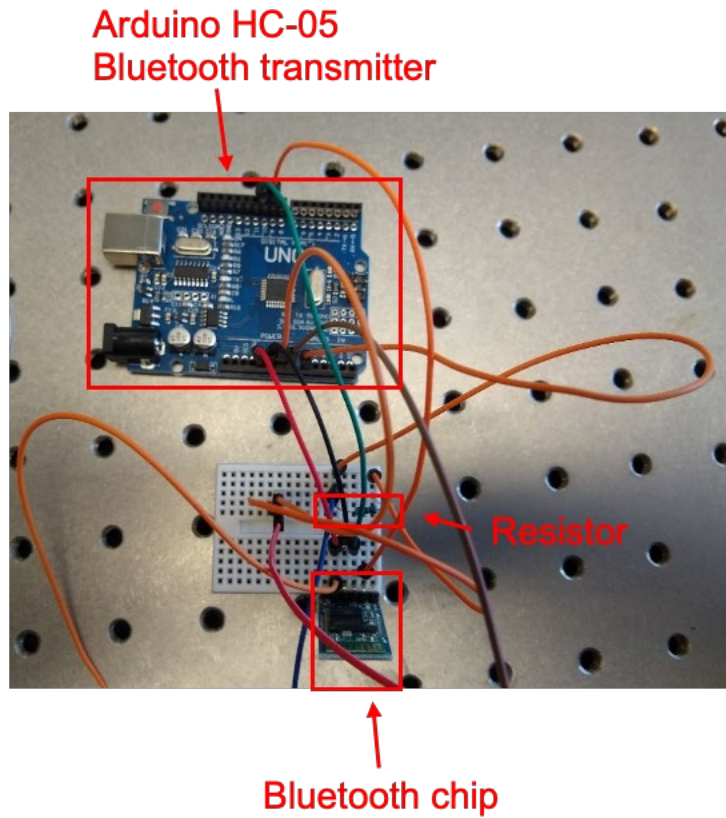Figure A.8 Piezoresistive sensing mechanism: dark lines are graphene
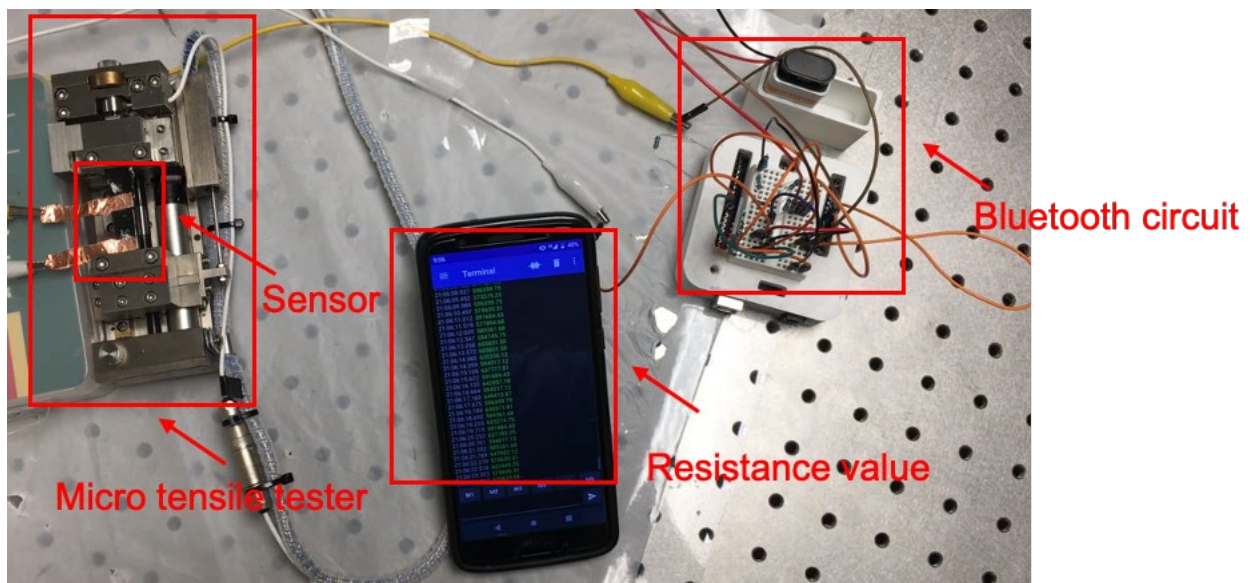
Figure A.9 Preliminary breadboard setup for DAQ

Figure A.10 Cellphone reading calibration using bluetooth